ChinaCropPhen1km: A high-resolution crop phenological dataset for three staple crops in China during 2000-2015 based on LAI products

Yuchuan Luo [1], Zhao Zhang [1*], Yi Chen [2], Ziyue Li [1], Fulu Tao [2, 3, *]

[1]State Key Laboratory of Earth Surface Processes and Resource Ecology/MEM&MoE Key Laboratory of Environmental Change and Natural Hazards, Faculty of Geographical Science, Beijing Normal University, Beijing 100875, China
[2]Key Laboratory of Land Surface Pattern and Simulation, Institute of Geographical Sciences and Natural Resources Research, Chinese Academy of Sciences, Beijing 100101, China
[3]College of Resources and Environment, University of Chinese Academy of Sciences, Beijing 100049, China

Correspondence to: Zhao Zhang (sunny_zhang@bnu.edu.cn)

Abstract. Crop phenology provides essential information for land surface phenology dynamics monitoring and modelling, and crop management and production. Most previous studies mainly investigated crop phenology at site scale, however, land surface phenology dynamics monitoring and modelling at a large-scale need a high-resolution spatially explicit information on crop phenology dynamics. In this study, we produced a 1km-grid crop phenological dataset for three main crops from 2000 to 2015 based on Global Land Surface Satellite (GLASS) Leaf Area Index (LAI) products, named as ChinaCropPhen1km. First, we compared three common smoothing methods and chose the most suitable one for different crops and regions. Then, we developed an optimal filter-based phenology detection (OFP) approach which combined both inflexion- and threshold-based method and detected the key phenological stages of three staple crops at 1km spatial resolution across China. Finally, we established a high resolution gridded-phenology product for three staple crops in China during 2000-2015. Compared with the intensive phenological observations from the Agricultural Meteorological Stations (AMS) of China Meteorological Administration (CMA), the dataset had a high accuracy with errors of retrieved phenological date less than 10 days, and represented the spatiotemporal patterns of the observed phenological dynamics at site scale fairly well. The well-validated dataset can be applied for many purposes including improving agricultural system or earth system modelling over a large area.
DOI of the referenced dataset: https://doi.org/10.6084/m9.figshare.8313530 (Luo et al., 2019).

1 Introduction

Phenology is a key indicator of vegetation growth and development and plays an important role in vegetation monitoring (Qiu et al., 2015;Tao et al., 2017;Zhong et al., 2016). Accurate information on the timing of key crop phenological stages is critical for determining the optimal timing of agronomic management options, reliable simulations of crop growth and yield, and analyzing the plant response to climate change (Bolton and Friedl, 2013;Brown et al., 2012;Chen et al., 2018a;Sakamoto et al., 2013;Sakamoto et al., 2010;Wang et al., 2015;Zhang and Tao, 2013).

30   Field phenological observations are time- and money-consuming. And the observational stations are limited and distributed sparsely. Therefore, the field phenological observations cannot meet the requirements of many purposes such as vegetation monitoring for remote areas with sparse observations and the grid-based earth system simulations. The satellite-based observations with a wide spatial coverage and short revisit times have become a powerful method to monitor vegetation growth and obtain vegetation information at regional and global scales. Previous studies have mainly used a vegetation index (VI) to

35   extract crop phenology. For examples, Pan et al. (2015) presented a method to construct Normalized Difference Vegetation Index (NDVI) time-series dataset derived from Environment and Disaster Monitoring and Prediction Satellite Constellation A/B (HJ-1 A/B) charge coupled device (CCD) sensor and extract phenology parameters. Zeng et al. (2016) detected corn and soybeans phenology with Moderate Resolution Imaging Spectroradiometer (MODIS) 250-m Wide Dynamic Range Vegetation Index (WDRVI) time-series data. Cao et al. (2015) developed an adaptive local iterative logistic fitting method to fit time-

40   series of Enhanced Vegetation Index (EVI) derived from MODIS and estimated green-up date of spring vegetation. Sakamoto (2018) refined the Shape Model Fitting method to estimate the timing of 36 crop-development stages of major U.S. crops from MODIS WDRVI time-series data. Crop phenology detected by these studies is relatively accurate. Nevertheless, it cannot be ignored that the VI are overly dependent on the band characteristics of sensors (Atzberger et al., 2014). By contrast, the Leaf Area Index (LAI) is more robust across diverse sensors and more sensitive than VI to large amounts of vegetation (Verger

45   et al., 2016). In addition, previous studies focused on only very limited areas or very few crops due to the high diversity and complexity of agricultural planting structures (Liao et al., 2019;Liu et al., 2017;Xu et al., 2017;Wang et al., 2012).

To implement a large-scale agricultural system simulation for multiple crops, there is an urgent need to acquire the gridded phenological dataset for each crop at a national or global scale. For example, crop model can simulate crop growth, development and predict crop yields. However, its applications to a large area are limited by the lack of accurate and spatially

50   heterogeneous crop growth information (Curnel et al., 2011;Dorigo et al., 2007;Tao et al., 2009;Jin et al., 2018). According to some previous studies, it could improve the accuracy of model estimation at large scale by assimilating reliable remote sensing data into crop growth models (Bolten et al., 2010;Nearing et al., 2012;Ines et al., 2013;Chen et al., 2018a;Huang et al., 2015;Zhou et al., 2019;de Wit and van Diepen, 2007). Among the state variables used in the assimilation, phenology is one of the essential variables because of its critical roles in affecting dry matter accumulation and distribution during the growing

55   stages and reflecting crop periodic biological changes influenced by various environmental conditions (e.g., climate) (Jin et al., 2018;Zheng et al., 2016).

In this study, using a remotely sensed Global Land Surface Satellite (GLASS) LAI product (2000-2015) (Xiao et al., 2014), we aim to 1) choose the most suitable smoothing method to reduce the noise of the LAI time-series for different crops and regions; 2) detect the phenological information of three staple crops (i.e., maize, rice and wheat) at 1-km spatial resolution

60   across China, and evaluate its accuracy by comparing with the observed data at Agricultural Meteorological Stations (AMS) of China Meteorological Administration (CMA); 3) explore the spatial patterns of different phenological stages. The resultant remote sensing LAI-based crop phenology dataset with 1-km spatial resolution across China (ChinaCropPhen1km) will benefit

to understand crop phenological dynamics, climate change impacts and adaptations, and agricultural system modelling over a large area, temporally and spatially (Luo et al., 2019).

65 **2 Data and methods**

2.1 Study area

The study areas across the mainland of China are characterized by complex environments and crop planting structures, diverse cropping intensity and cultivation habits (Fig. 1-a) (Piao et al., 2010;Zhang et al., 2014a). Additionally, we divided the whole study areas into different subregions for each crop based on the cropping system and growth environment (Fig. 1-b, c, d). More

70 details of the subregions for each crop were shown in Table S1-S3. Rice, wheat and maize are the three staple crops in China, together accounting for 59% of the total planting area and 92% of the grain yield in 2017. Roughly half of the cropland in China is multi-cropped, such as the double cropping system of wheat-maize in the North China Plain, and the rotation system between early-rice and late rice in Southern China (Frolking et al., 2002).

2.2 Data

75 **2.2.1 ChinaCropPhen1km input data**

An improved MODIS-based LAI dataset (GLASS LAI) from 2000 to 2015 was from Liang et al. (2013) (http://glass-product.bnu.edu.cn/?pid=3&c=1). The GLASS LAI product was generated with general regression neural networks (GRNNs) trained by the fused LAI from MODIS and Carbon cYcle and Change in Land Observational Products from an Ensemble of Satellites (CYCLOPES) LAI products and the reprocessed MODIS reflectance of the BEnchmark Land Multisite ANalysis

80 and Intercomparison of Products (BELMANIP) sites during the period 2001-2003 (Liang et al., 2013). By computing the Root Mean Square Error (RMSE) and determination coefficients (R^2) between several global LAI products and the high-resolution LAI reference map, it could be shown that the accuracy of the GLASS LAI (RMSE=0.78, R^2=0.81) was fairly better than that of the MODIS LAI product (MOD15) and Geoland2/BioPar version 1 (GEOV1) (Xiao et al., 2016). Moreover, the intercomparison have indicated that GLASS LAI (8-day composites of 1-km spatial resolution) was more temporally

85 continuous and spatially complete than the other LAI products (Xiao et al., 2014;Xiao et al., 2016). It has been applied to vegetation monitoring and crop model assimilation (Xiao et al., 2014;Chen et al., 2018a).

In addition, the cultivated-land layer derived from the 1-km National Land Cover Dataset (NLCD) of China was used as cropland masks. Specifically, we detected the key phenological dates for dryland crops (i.e., maize and wheat) and paddy rice, which were restricted on the dry land and paddy field layer derived from the NLCD, respectively. NLCD was provided by

90 Data Centre for Resources and Environmental Sciences, Chinese Academy of Sciences (http://www.resdc.cn/Default.aspx), which also included several epochs of land use datasets, i.e., 2000, 2005, 2010 and 2015 (Liu et al., 2005;Liu et al., 2014).

2.2.2 ChinaCropPhen1km validation data

The crop phenology observation records from 2000 to 2013 of maize, rice, and wheat crops were obtained from AMS, which were governed by CMA (https://data.cma.cn/). Such phenology information was observed and recorded by well-trained agricultural technicians in the experimental field, and then checked and managed by the Chinese Agricultural Meteorological Monitoring System (CAMMS). In this study, we selected the agrometeorological stations with more than 10 years of records of key phenological dates, including green-up date, emergence date, transplanting date, V3 stage (i.e., early vegetative stage of maize when the third leaf is fully expanded), heading date, and maturity date, for the three crops. Totally, there were 436 stations across main crop-cultivated areas in China (Fig. 1).

2.3 Methods

The method to retrieve the phenological information of three staple crops at national scale is presented schematically in Fig. 2. The data processes are as follows: 1) data preprocessing, 2) selecting the cropland sample grid to determine the suitable smoothing method, 3) determining the optimal filter-based phenology detection (OFP) approach, 4) generating ChinaCropPhen1km dataset.

2.3.1 Data preprocessing

Due to the differences among these datasets on projected coordinate system, firstly, we projected or re-projected all raster data to "Asia North Albers Equal Area Conic" by using the Projection Raster tool in ArcGIS. Then, we combined 46 annual GLASS LAI images together and used a China provincial administrative vector map to mask images by province. Finally, a LAI time-series was created for each pixel for further applications.

2.3.2 ChinaCropPhen1km LAI smoothing methods

Previous studies have proposed different smoothing methods to reduce the noise of GLASS LAI time series, and found the OFP method varied by studied times, areas, and objectives (Zhao et al., 2016;Wang et al., 2018). Three commonly used methods were chosen in the study to smooth the LAI time-series curves, including the Double Logistic (DL) method, Savitzky-Golay (S-G) filter method, and Wavelet-based filter (WF) method.

2.3.2.1 Double logistic (DL) method

Double logistic is a method of merging local fitting parts to obtain the overall fitting result (Jonsson and Eklundh, 2004). In the local fitting process, the Double logistic function can be expressed as:

$$g(t; x_1, ..., x_4) = \frac{1}{1 + exp(\frac{x_1 - t}{x_2})} - \frac{1}{1 + exp(\frac{x_3 - t}{x_4})} \qquad (1)$$

where, x_1 determines the position of the left inflection point while x_2 gives the rate of change. Similarly, x_3 determines the position of the right inflection point while x_4 gives the rate of change at this point.

2.3.2.2 Savitzky-Golay (S-G) filter method

Based on locally adaptive moving window, Savitzky-Golay (S-G) filtering method can be used to smooth data and suppress disturbances with a local polynomial regression model (Savitzky and Golay, 1964). Algorithm can be summarized as follows:

$$LAI_j^* = \frac{\sum_{i=-n}^{i=n} C_i LAI_{j+i}}{N} \tag{2}$$

where, LAI_{j+i} represents the original LAI value, LAI_j^* is the smoothed LAI value, j is running index of the LAI time series, C_i is the coefficient of the i-th LAI value, n is the half-width of the smoothing window, and N is the width of the moving window to perform filtering (2n+1). The width of the moving window—N, not only determines the degree of smoothing, but also affects the ability to follow a rapid change. We selected three windows width (3, 4, 5) to identify a better width for different crops and regions.

2.3.2.3 Wavelet-based filter (WF) method

Wavelet-based filter method can reduce noise with reflecting the periodicity of seasonal vegetation change (Sakamoto et al., 2005). The input signals $f(x)$ is transformed in the wavelet transform as follows:

$$Wf(a,b)_i = \frac{1}{\sqrt{a}} \int \varphi(\frac{x-b}{a}) f(x) dx \tag{3}$$

where a is a scaling parameter, b is a shifting parameter, and φ implies a mother wavelet.

The advantage of the WF method is that it can maintain the time components of time-series data and hardly distort signals. The input signals $f(x)$ is decomposed to linear combinations of wavelet functions in the multi-resolution approximation:

$$f(x) = \sum_{i=1}^{j} [f(x)_i + g(x)_i] \tag{4}$$

where $f(x)_i$ implies the approximate expression in level i, and $g(x)_i$ implies the high-frequency components in level i. We used three types of mother wavelets: Daubechies (1988) (order=3–24), Coiflet (order=1–5), and Symlet (order=4–15) in the study.

2.3.3 Methods to detect the phenological information

The methods to detect remote-sensing-based phenology can generally be classified into three groups: inflexion-based method (Chen et al., 2016), threshold-based method (Manfron et al., 2017), and methods based on the mathematical or geometrical model fitting approach (Sakamoto et al., 2010). In this study, we used both inflexion- and threshold-based methods together

to detect phenology. Firstly, we defined the inflection and maximum points of LAI time-series as the specific timing of key phenological stages for different crops (Fig. 3).

2.3.3.1 Green-up date, emergence date, transplanting date and V3 stage

We defined the date of inflection point (the first derivative increases continuously after this point or the second derivative equals 0) of the LAI time-series curves as the green-up date of winter wheat, emergence date of spring wheat, transplanting date of rice and V3 stage (early vegetative stage of maize when the third leaf is fully expanded) of maize (Sakamoto, 2018;Sakamoto et al., 2005;Sakamoto et al., 2010). Before the inflection point, the LAI values are kept low for a long time, and then they start to increase continuously after this point.

2.3.3.2 Heading date

Heading date in the study was defined as the day when LAI reaching the maximum, as similar as some previous studies (Sakamoto et al., 2005;Chen et al., 2018b). That is to say, the maximum LAI points in the time-series curve are regarded as the heading dates.

2.3.3.3 Maturity date

When crops reach maturity, the physiological activity will change largely, leading to an abrupt decrease in LAI (Sakamoto et al., 2005;Chen et al., 2018b). Therefore, we regarded an inflection point in the LAI time-series curve, where the first derivative is negative with the largest absolute value, as the maturity date.

2.3.4 Determining the optimal filter-based phenology detection approach (OFP)

Based on the observations around the nearest AMS, we needed firstly to determine the restricted time windows responding to each key phenological stage for different crops. Then we sampled randomly 1000 grids every year in each province from the grids where the land use data was identified as cropland and retrieved the key phenological stages in the sampling grids according to the three smoothing methods and the above definitions of key stages. To determine the OFP approach in each province, we identified the inflection points and maximum value point of each LAI time-series curve at each grid within the restricted time windows. After detecting phenological information of the cropland sample grids, we calculated the RMSE values between the estimated phenological dates and observed dates, and averaged these RMSE values for each crop at a provincial scale. Finally, we chose the most suitable smoothing method for different crops in each province with minimum RMSE.

2.3.5 Generating ChinaCropPhen1km dataset

After removing the grids from where the land use data was identified as non-cropland, we then obtained cropland grids where the phenological information will be detected. Then, the most suitable smoothing method for different crops in each province were applied to reconstruct the LAI time series at 1-km grid scale. Finally, we detected the key phenological dates using OFP approach and determined the cultivated grids for each crop on the basis of three key phenological stages could be identified simultaneously. For example, if the green-up date, heading date and maturity date (corresponding to the inflection and maximum points in LAI time-series) of winter wheat could be simultaneously detected for a specific grid, then it could be regarded as the cultivated grid of winter wheat. Additionally, to evaluate the accuracy of the estimated phenological dates at a national scale, we calculated the mean of phenological dates detected from each crop pixel around corresponding AMS and compared them with the corresponding observations by using RMSE.

3 Results and Discussion

3.1 Comparisons of different smoothing methods

The smoothed time profiles of LAI generated by different smoothing methods are shown in Fig. 4. Both S-G filter and WF method can smooth LAI time-series well. That is to say, the generated time profiles of LAI match well with the seasonal tendency of the observed LAI time-series in the field. In addition, both methods can clearly characterize the local changes in the time component and maintain the time components of LAI time-series data. Although DL method performs poorly for smoothing LAI time series of the double-season crops, it is still reliable for single-season crops. These findings were consistent with those in some previous studies (Zhu et al., 2012;Sakamoto et al., 2005;Qiu et al., 2016).

We further compared mean RMSE of different smoothing methods and selected the most suitable smoothing method with minimal mean RMSE for different provinces and crops (Table 1). If the RMSE values were same, we also compared the number of crop grids according to different smoothing methods, and selected the suitable method which had identified a larger number of crop girds. It is noted that the number of identified grids differ considerably even with same RMSE values. Totally, S-G filter was an overwhelming smoothing way for 95% crops and provinces, followed by WF and DL method.

We ascribed the great performance of S-G to two reasons as follows. 1) One is its scientific smoothing principle: S-G filter applies an iterative weighted moving average filter to the time series, which can replace the noise data as well as keep the fidelity (Geng et al., 2014). By contrast, WF decomposes the time series into scaled and shifted wavelets to acquire time-localization of a given signal (Qiu et al., 2014). DL uses a series of parameters to fit the time series (Beck et al., 2006). 2) The other is that S-G is more suitable for GLASS LAI. S-G can catch the local variations—e.g. the bimodal curve characteristics from double cropping rice and the rotation of winter wheat and summer maize (Fig. 3-b, f) — in time series and perform best for data without extreme noise such as GLASS LAI (Eklundh and Jönsson, 2015). DL is more useful for data with much noise, however, fails to catch local changes due to being unfit for data with double peaks. WF is also a powerful tool for processing

non-stationary and noisy signals such as VI time-series rather than GLASS LAI (Rouyer et al., 2008; Sakamoto et al., 2006). Therefore, S-G is the most suitable for the complex cultivating systems across whole mainland of China. We also attributed the excellent performance of S-G to the phenological extraction rules established in this paper, and the goal of accurately extracting the crop cultivation grids, as well as key phenology stages. For example, WF smoothing method might eliminate pseudo inflexion points that may not be pseudo due to the uncertainty of GLASS LAI data sometimes, and misidentify non-crop grids by inflexion- and threshold-based methods consequently resulting in very few crop grids identified (Qiu et al., 2016).

3.2 Validation of ChinaCropPhen1km

The comparison between retrieved phenological dates and phenological observations of each crop from 2000-2015 at national scale showed that all retrieved and observed dates were closely and averagely distributed 1:1 line for three crops (Fig. 5). Additionally, the RMSE values of retrieved phenological dates were consistently less than 10 days (Table 2). The RMSE averages of three key dates for rice were around 5.3 days, followed by wheat (5.5 days) and maize (6.7 days), corresponding to the related R^2 of 0.98, 0.97 and0.97, respectively.

As for the differences among crops, the retrieved accuracy of maize phenological stages was consistently the worst, with the biggest RMSE and errors ($\geq\pm10$ days), and the lowest errors ($\leq\pm10$ days) and R^2. We ascribed the lower accuracy of maize phenology to the wider spatial heterogeneity environment and the complex rotation planting system relative to the other two crops (Qiu et al., 2018). The highest accuracy of rice phenology also supported the accuracy impact of complex planting system because paddy field is unfit for dryland crops such as maize, wheat, soybean, and other coarse cereals (Dong et al., 2015).

More interestingly, the retrieved accuracy of three crops decreased as crop growing and developing up to maturity periods (Table 2), with the average RMSEs ranging from 3.7 to 7.2 days. The highest accuracy (RMSE=2.8, error=0.5%) was found for the green up/emergence stages of wheat, while accuracy of maturity stage for each crop were the lowest (average RMSE=7.2, error=19%). The reasonable explanation might be relative weaker interfere from other vegetation because the green-up/emergence stage occurs most early during plant growing period (some 80 DOY Table 3). With the land surface greening up, more and more information on plant growing statuses will be shot by satellites, which consequently mix with the crops' information and interfere to retrieve accurately the phenological stages of crops. Of course, the interfering from anthropological activities should not be ignored with climate warming.

Nevertheless, overall the retrieved phenological dates for the three crops are in strong correspondence with the observational dates ($R^2 > 0.95$) and their relationships are statistically significant (p < 0.01). Meanwhile, the growing status of other plants (or rotation crops e.g. wheat-maize, maize-soybean) and the influence of other noises will lead to deviations of the remote-sensing LAI curve and the actual observed curve in the field. The noises also include other factors, e.g. weather conditions, farmers' behaviors, etc... However, the uncertainty does not exclude the applicability of our method to retrieve key phenological stages of crops, especially retrieving relative higher resolution phenological information based on mature remote-sensing products at a large spatial scale.

3.3 Spatiotemporal patterns of key phenological stages from 2000 to 2015

235 We showed the annual averages of each key crop growth stage to indicate their spatiotemporal patterns due to the similarity in inter-annual patterns for a certain crop over the 16 years (Figs.6-7, Table 3, and Fig. S1-S4). Besides summarizing the key stages by crops and sub-regions, we also calculated three crop growth periods, including VGP (vegetative growth period), RGP (reproductive growth period) and GP$_W$ (whole growth period) to interpret their patterns (Fig.8, Table 3). Among the five sub-regions with rice cultivation, the sub-region III was the most complex because three types of rice were cultivated there

240 (Fig.6-a; Fig.7-a). The single-rice in the sub-region III was generally cultivated in the northern parts of four provinces (i.e., Anhui, Jiangsu, Zhejiang and Hubei), which was characterized by three key stages occurring latest (DOY 159~265) than other three single-rice sub-regions (I, II, IV). Moving from the south (IV) to north (I) (excluding the sub-region III because of cultivation of double-rice), single-rice was not transplanted in sequence as expected. In the sub-region II, it was transplanted latest (DOY 154) but had relatively early maturity dates (DOY 255), resulting in the shortest growing period (101 days) (Fig.8-

245 a). On the contrary, in the sub-region IV, single-rice was transplanted earliest but had the maturity occurring latest, resulting in the longest growing period of 130 days (Figs.6-a, 7-a, 8-a). In the sub-region V where only double rice was cultivated, early-rice was transplanted earlier (DOY 99), maturity dates of late rice occurred later (DOY 310), and consequently resulting in longer growing periods (97 and 101 days for corresponding early and late-rice) than those in the sub-region III with double-rice cultivation (80 and 84 days) (Table 3).

250 As for wheat, green-up & emergence dates ranged most widely (DOY 30~128) than other crops. Winter wheat in the sub-regions II and IV had earlier green-up dates, while spring wheat in the sub-regions of I and III had later emergence dates (Table 3, Figs.6-b, 7-b). Moreover, along with the latitudes from the north to south (excluding the sub-region III because of the sparsest wheat cultivation there), the first key dates became earlier but with shorter growth periods (106, 93, 92 days for I, II and IV) due to the sufficient temperature and light in the sub-region IV (Yu et al., 2012) (Fig.8-b). Interestingly, the heading

255 and maturity dates in the three sub-regions showed consistently the same spatial patterns as that of the first stage with latitudes decreasing (Figs.6-b, 7-b).

Both spring and summer maize types were concurrently cultivated in the sub-regions III and IV, while only one of them was cultivated in the sub-regions I and II, the main planting areas of northern China (Figs. 6-c, Fig.7-c, Table 3). V3 of summer maize was approximately 43 days later than that of spring maize (DOY 161 vs. 117), but their maturity dates were very close

260 (DOY 259 vs. 245), which thus caused a shorter growth period for summer maize, especially for the sub-regions II and III (some 84 days) (Fig.8-c). Additionally, in three sub-regions (I, III, IV) for spring maize, like wheat, the spatial patterns of the three key stages for maize were similar in spatial patterns with latitude increasing. Finally, the key dates and periods were the most variable in the sub-region IV (Figs.7-c, 8-c).

In sum, the spatial patterns of key phenological stages varied by crops and cultivated ways. In addition, early rice and single

265 cropping rice in the sub-region III, wheat in the sub-region III, and maize and rice in the sub-region IV showed a larger variability than others due to the mixed planting of heterogeneous varieties of the same crop. Many factors could have impacts

on crop phenology, such as climate, environment, farmer's behaviors, technological development, and human activities (Liu et al., 2016;Liu et al., 2018). Different from natural ecosystems such as wild forest or grassland, three main crops cultivated across the mainland of China did not reach greening-up or flowering dates in sequence with latitude, especially for rice (Zhang et al., 2015;Tao et al., 2014;Zhang et al., 2014b). Moreover, climate conditions did have impacts on crop phenology. For example, increased temperature had advanced heading and maturity date of crops in China (He et al., 2015;Tao et al., 2014). At the same time, crop management activities, such as cultivar shift and the adjustment of planting and harvesting date, had affected crop phenology largely (Tao et al., 2006;Tao et al., 2013).

3.4 The changes in three key phenological dates and growth periods from 2000 to 2015

To interpret the changes of the three key phenological dates and growth periods from 2000 to 2015, we analyzed their trends at pixel scale and summarized the grids with a significant trend ($p<0.1$) according to crops and sub-regions (Figs 9-10, Table 4). We found more positive trends, with 0.78 days/year for 70% summarized medians, but fewer negative ones, with -0.69 days/year and 30% medians. This suggests that phenological dates have been delayed. Specifically, the proportion of pixels that had a positive trend is 92% for wheat (Fig.9-b), 75% for rice (Fig.9-a), and 50% for maize (Fig.9-c).

For rice, transplanting dates were consistently advanced by -0.64 days/year for early rice and single-rice, and delayed by 0.84 days/year for late rice in most areas. Maturity dates became later by 1.23 days/year, but heading dates had less changes. In addition, double rice in the sub-region III showed less variable than that in the sub-region V (Fig.9-a). By contrast, the first stages (i.e., green-up & emergence) delayed by 0.88 days/year consistently for almost all the wheat cultivation areas (Fig.9-b). Maize in the sub-region II, and wheat in the sub-region I and II (Fig.9-b), had an opposite trend to that of rice (Fig.9, Table 4).

Moreover, the changes in the three stages showed less variable in the sub-region II, the main planting areas for both dryland crops. Among all the crops and growth stages, maize in the regions III and IV had consistently negative trends with exception of maturity dates in the sub-region IV.

Compared with the significant changes in phenological dates, the duration of phenological periods changed in less pixels (< 30%) (Table 4). More pixels with positive trends, with 1.25 days/year for 66.7% medians, were identified than those with negative trends, with -0.97 days/year for 32.3% medians, implying a commonly prolonged growth periods during the study period. 95.8% of the medians were positive for rice, while 75% of the medians were negative for wheat. The changes of maize growth periods were similar to those of its phenological dates.

The duration of growth periods was prolonged, especially for the whole growth period (GPw), which was consistently observed for rice cropping systems, except for early rice in the sub-region V. In addition, the duration of VGP for single rice in the sub-region I had weaker trends (Fig. 10-a). On the contrary, almost all the wheat growth periods were shortened except for winter wheat in the sub-region V, especially for spring wheat in the sub-region I (Fig.10-b). Additionally, in term of growth period duration, maize had the similar changes as wheat in the sub-regions I and II. Changes in growth period duration were different for spring (shortened) and winter (prolonged) wheat, and for both maize types between the sub-region III and IV (Fig.10-c).

The results are well supported by some previous studies based on the intensive observations at site scale (Tao et al., 2013;Tao et al., 2014;Tao et al., 2012;Zhang et al., 2014b).

3.5 Uncertainties of ChinaCropPhen1km

Inevitably, there are still uncertainties in the generated dataset (i.e., ChinaCropPhen1km). On the one hand, GLASS LAI products might lead to some uncertainties in ChinaCropPhen1km. First of all, the noise of original GLASS LAI time-series could reduce the accuracy of detected phenological stages, which was resulted from many factors such as cloud, snow, aerosols, and water vapor (Xiao et al., 2014). Therefore, we compared several commonly used smoothing methods and chose the most suitable one with minimum RMSE for different crops in each province, which could reduce some uncertainties. Moreover, the GLASS LAI retrieval algorithm eliminates abrupt spikes and dips, which may result in the loss of neighboring smaller peaks in LAI profiles (Xiao et al., 2016). The number of detected pixels with double-season rice cultivated might be less than that of the actual situation due to the short interval between the two local maximum points (i.e., heading stages of early rice and late rice) (Fig. 3-f). On the other hand, mixed pixel might bring uncertainty in the results as it contained several land cover types and then weakened the identified signal of specific phenological stages. We ascribed the occurrence of mixed pixel to two reasons. One is the coarse spatial resolution of 1 km. For example, mixed pixel occurs widely in the mountainous regions (e.g., southern China) with complex terrain and diverse vegetation types. The other is that we determined the spatial distribution of each dryland crop (i.e., maize and wheat) based on the dryland layer of NLCD, which might include several crop types. In future studies, the application of crop-specific map and remote sensing products with finer spatial resolution is expected to solve the mixed pixel issues.

4 Data availability

The derived crop phenological dataset for three staple crops in China during 2000-2015 is available at https://doi.org/10.6084/m9.figshare.8313530 (Luo et al., 2019).

5 Conclusion

In the present study, we generated 1km-grid crop phenological dataset for three main crops from 2000 to 2015 based on GLASS LAI products, named as ChinaCropPhen1km. First, we compared three common smoothing methods and chose the most suitable one for different crops and regions. The results showed that S-G was the most frequently chosen method as it not only could well smooth the time series but also keep the fidelity. Next, we developed an OFP approach which combined both inflexion- and threshold-based method to detect the key phenological stages of three staple crops at spatial resolution of 1km across China. Finally, we established a high resolution gridded-phenology product for three staple crops in China during 2000-2015.

The ChinaCropPhen1km dataset has been well validated using the intensive phenological observations of AMS, which substantiates a high accuracy with errors of retrieved phenological date less than 10 days. It can reflect the spatial differences in the local climatic and management factors. Thus, this first high-resolution crop phenological dataset can be applied for many purposes, including understanding land surface phenological dynamics, investigating climate change impacts and adaptations, and improving agricultural system or earth system modelling over a large area, temporally and spatially.

Author contribution

Zhao Zhang and Yi Chen designed the research. Yi Chen and Ziyue Li collected datasets. Yuchuan Luo implemented the research and wrote the paper; Zhao Zhang and Fulu Tao revised the manuscript.

Competing interests

The authors declare that they have no conflict of interest.

Acknowledgements

This study was funded by National Basic Research Program of China (41977405, 41571493, 41571088, 31561143003), and State Key Laboratory of Earth Surface Processes and Resources Ecology.

References

Atzberger, C., Klisch, A., Mattiuzzi, M., and Vuolo, F.: Phenological Metrics Derived over the European Continent from NDVI3g Data and MODIS Time Series, Remote Sens-Basel, 6, 257-284, https://doi.org/10.3390/rs6010257, 2014.

Beck, P. S. A., Atzberger, C., Hogda, K. A., Johansen, B., and Skidmore, A. K.: Improved monitoring of vegetation dynamics at very high latitudes: A new method using MODIS NDVI, Remote Sens Environ, 100, 321-334, https://doi.org/10.1016/j.rse.2005.10.021, 2006.

Bolten, J. D., Crow, W. T., Zhan, X. W., Jackson, T. J., and Reynolds, C. A.: Evaluating the Utility of Remotely Sensed Soil Moisture Retrievals for Operational Agricultural Drought Monitoring, Ieee J-Stars, 3, 57-66, https://doi.org/10.1109/Jstars.2009.2037163, 2010.

Bolton, D. K., and Friedl, M. A.: Forecasting crop yield using remotely sensed vegetation indices and crop phenology metrics, Agr Forest Meteorol, 173, 74-84, https://doi.org/10.1016/j.agrformet.2013.01.007, 2013.

Brown, M. E., de Beurs, K. M., and Marshall, M.: Global phenological response to climate change in crop areas using satellite remote sensing of vegetation, humidity and temperature over 26 years, Remote Sens Environ, 126, 174-183, https://doi.org/10.1016/j.rse.2012.08.009, 2012.

355   Cao, R. Y., Chen, J., Shen, M. G., and Tang, Y. H.: An improved logistic method for detecting spring vegetation phenology in grasslands from MODIS EVI time-series data, Agr Forest Meteorol, 200, 9-20, https://doi.org/10.1016/j.agrformet.2014.09.009, 2015.

Chen, Y., Zhang, Z., and Tao, F. L.: Improving regional winter wheat yield estimation through assimilation of phenology and leaf area index from remote sensing data, Eur J Agron, 101, 163-173, https://doi.org/10.1016/j.eja.2018.09.006, 2018a.

360   Chen, Y., Zhang, Z., Tao, F. L., Palosuo, T., and Rotter, R. P.: Impacts of heat stress on leaf area index and growth duration of winter wheat in the North China Plain, Field Crop Res, 222, 230-237, https://doi.org/10.1016/j.fcr.2017.06.007, 2018b.

Chen, Y. L., Song, X. D., Wang, S. S., Huang, J. F., and Mansaray, L. R.: Impacts of spatial heterogeneity on crop area mapping in Canada using MODIS data, Isprs J Photogramm, 119, 451-461, https://doi.org/10.1016/j.isprsjprs.2016.07.007, 2016.

365   Curnel, Y., de Wit, A. J. W., Duveiller, G., and Defourny, P.: Potential performances of remotely sensed LAI assimilation in WOFOST model based on an OSS Experiment, Agr Forest Meteorol, 151, 1843-1855, https://doi.org/10.1016/j.agrformet.2011.08.002, 2011.

Daubechies, I.: Orthonormal Bases Of Compactly Supported Wavelets, Commun Pur Appl Math, 41, 909-996, https://doi.org/10.1002/cpa.3160410705, 1988.

370   de Wit, A. M., and van Diepen, C. A.: Crop model data assimilation with the Ensemble Kalman filter for improving regional crop yield forecasts, Agr Forest Meteorol, 146, 38-56, https://doi.org/10.1016/j.agrformet.2007.05.004, 2007.

Dong, J. W., Xiao, X. M., Kou, W. L., Qin, Y. W., Zhang, G. L., Li, L., Jin, C., Zhou, Y. T., Wang, J., Biradar, C., Liu, J. Y., and Moore, B.: Tracking the dynamics of paddy rice planting area in 1986-2010 through time series Landsat images and phenology-based algorithms, Remote Sens Environ, 160, 99-113, https://doi.org/10.1016/j.rse.2015.01.004, 2015.

375   Dorigo, W. A., Zurita-Milla, R., de Wit, A. J. W., Brazile, J., Singh, R., and Schaepman, M. E.: A review on reflective remote sensing and data assimilation techniques for enhanced agroecosystem modeling, Int J Appl Earth Obs, 9, 165-193, https://doi.org/10.1016/j.jag.2006.05.003, 2007.

Eklundh, L., and Jönsson, P.: TIMESAT: A Software Package for Time-Series Processing and Assessment of Vegetation Dynamics, in, 141-158, https://doi.org/ 10.1007/978-3-319-15967-6_7, 2015.

380   Frolking, S., Qiu, J. J., Boles, S., Xiao, X. M., Liu, J. Y., Zhuang, Y. H., Li, C. S., and Qin, X. G.: Combining remote sensing and ground census data to develop new maps of the distribution of rice agriculture in China, Global Biogeochem Cy, 16, Artn 1091, https://doi.org/10.1029/2001gb001425, 2002.

Geng, L. Y., Ma, M. G., Wang, X. F., Yu, W. P., Jia, S. Z., and Wang, H. B.: Comparison of Eight Techniques for Reconstructing Multi-Satellite Sensor Time-Series NDVI Data Sets in the Heihe River Basin, China, Remote Sens-Basel, 6, 385   2024-2049, https://doi.org/10.3390/rs6032024, 2014.

He, L., Asseng, S., Zhao, G., Wu, D. R., Yang, X. Y., Zhuang, W., Jin, N., and Yu, Q.: Impacts of recent climate warming, cultivar changes, and crop management on winter wheat phenology across the Loess Plateau of China, Agr Forest Meteorol, 200, 135-143, https://doi.org/10.1016/j.agrformet.2014.09.011, 2015.

390 Huang, J. X., Ma, H. Y., Su, W., Zhang, X. D., Huang, Y. B., Fan, J. L., and Wu, W. B.: Jointly Assimilating MODIS LAI and ET Products Into the SWAP Model for Winter Wheat Yield Estimation, Ieee J-Stars, 8, 4060-4071, https://doi.org/10.1109/Jstars.2015.2403135, 2015.

Ines, A. V. M., Das, N. N., Hansen, J. W., and Njoku, E. G.: Assimilation of remotely sensed soil moisture and vegetation with a crop simulation model for maize yield prediction, Remote Sens Environ, 138, 149-164, https://doi.org/10.1016/j.rse.2013.07.018, 2013.

395 Jin, X. L., Kumar, L., Li, Z. H., Feng, H. K., Xu, X. G., Yang, G. J., and Wang, J. H.: A review of data assimilation of remote sensing and crop models, Eur J Agron, 92, 141-152, https://doi.org/10.1016/j.eja.2017.11.002, 2018.

Jonsson, P., and Eklundh, L.: TIMESAT - a program for analyzing time-series of satellite sensor data, Comput Geosci-Uk, 30, 833-845, https://doi.org/10.1016/j.cageo.2004.05.006, 2004.

Liang, S. L., Zhao, X., Liu, S. H., Yuan, W. P., Cheng, X., Xiao, Z. Q., Zhang, X. T., Liu, Q., Cheng, J., Tang, H. R., Qu, Y.
400 H., Bo, Y. C., Qu, Y., Ren, H. Z., Yu, K., and Townshend, J.: A long-term Global LAnd Surface Satellite (GLASS) data-set for environmental studies, Int J Digit Earth, 6, 5-33, https://doi.org/10.1080/17538947.2013.805262, 2013.

Liao, C. H., Wang, J. F., Dong, T. F., Shang, J. L., Liu, J. G., and Song, Y.: Using spatio-temporal fusion of Landsat-8 and MODIS data to derive phenology, biomass and yield estimates for corn and soybean, Sci Total Environ, 650, 1707-1721, https://doi.org/10.1016/j.scitotenv.2018.09.308, 2019.

405 Liu, J. Y., Liu, M. L., Tian, H. Q., Zhuang, D. F., Zhang, Z. X., Zhang, W., Tang, X. M., and Deng, X. Z.: Spatial and temporal patterns of China's cropland during 1990-2000: An analysis based on Landsat TM data, Remote Sens Environ, 98, 442-456, https://doi.org/10.1016/j.rse.2005.08.012, 2005.

Liu, J. Y., Kuang, W. H., Zhang, Z. X., Xu, X. L., Qin, Y. W., Ning, J., Zhou, W. C., Zhang, S. W., Li, R. D., Yan, C. Z., Wu, S. X., Shi, X. Z., Jiang, N., Yu, D. S., Pan, X. Z., and Chi, W. F.: Spatiotemporal characteristics, patterns, and causes of land-
410 use changes in China since the late 1980s, J Geogr Sci, 24, 195-210, https://doi.org/10.1007/s11442-014-1082-6, 2014.

Liu, Q., Fu, Y. S. H., Zhu, Z. C., Liu, Y. W., Liu, Z., Huang, M. T., Janssens, I. A., and Piao, S. L.: Delayed autumn phenology in the Northern Hemisphere is related to change in both climate and spring phenology, Global Change Biol, 22, 3702-3711, https://doi.org/10.1111/gcb.13311, 2016.

Liu, Y. J., Chen, Q. M., Ge, Q. S., Dai, J. H., Qin, Y., Dai, L., Zou, X. T., and Chen, J.: Modelling the impacts of climate
415 change and crop management on phenological trends of spring and winter wheat in China, Agr Forest Meteorol, 248, 518-526, https://doi.org/10.1016/j.agrformet.2017.09.008, 2018.

Liu, Z. J., Wu, C. Y., Liu, Y. S., Wang, X. Y., Fang, B., Yuan, W. P., and Ge, Q. S.: Spring green-up date derived from GIMMS3g and SPOT-VGT NDVI of winter wheat cropland in the North China Plain, Isprs J Photogramm, 130, 81-91, https://doi.org/10.1016/j.isprsjprs.2017.05.015, 2017.

420 Luo, Y., Zhang, Z., Chen, Y., Li, Z. and Tao, F.: ChinaCropPhen1km: A high-resolution crop phenological dataset for three staple crops in China during 2000-2015 based on LAI products, https://doi.org/10.6084/m9.figshare.8313530, 2019.

Manfron, G., Delmotte, S., Busetto, L., Hossard, L., Ranghetti, L., Brivio, P. A., and Boschetti, M.: Estimating inter-annual variability in winter wheat sowing dates from satellite time series in Camargue, France, Int J Appl Earth Obs, 57, 190-201, https://doi.org/10.1016/j.jag.2017.01.001, 2017.

425   Nearing, G. S., Crow, W. T., Thorp, K. R., Moran, M. S., Reichle, R. H., and Gupta, H. V.: Assimilating remote sensing observations of leaf area index and soil moisture for wheat yield estimates: An observing system simulation experiment, Water Resour Res, 48, Artn W05525, https://doi.org/10.1029/2011wr011420, 2012.

Pan, Z. K., Huang, J. F., Zhou, Q. B., Wang, L. M., Cheng, Y. X., Zhang, H. K., Blackburn, G. A., Yan, J., and Liu, J. H.: Mapping crop phenology using NDVI time-series derived from HJ-1 A/B data, Int J Appl Earth Obs, 34, 188-197, 430   https://doi.org/10.1016/j.jag.2014.08.011, 2015.

Piao, S. L., Ciais, P., Huang, Y., Shen, Z. H., Peng, S. S., Li, J. S., Zhou, L. P., Liu, H. Y., Ma, Y. C., Ding, Y. H., Friedlingstein, P., Liu, C. Z., Tan, K., Yu, Y. Q., Zhang, T. Y., and Fang, J. Y.: The impacts of climate change on water resources and agriculture in China, Nature, 467, 43-51, https://doi.org/10.1038/nature09364, 2010.

Qiu, B. W., Zhong, M., Tang, Z. H., and Wang, C. Y.: A new methodology to map double-cropping croplands based on 435   continuous wavelet transform, Int J Appl Earth Obs, 26, 97-104, https://doi.org/10.1016/j.jag.2013.05.016, 2014.

Qiu, B. W., Li, W. J., Tang, Z. H., Chen, C. C., and Qi, W.: Mapping paddy rice areas based on vegetation phenology and surface moisture conditions, Ecol Indic, 56, 79-86, https://doi.org/10.1016/j.ecolind.2015.03.039, 2015.

Qiu, B. W., Feng, M., and Tang, Z. H.: A simple smoother based on continuous wavelet transform: Comparative evaluation based on the fidelity, smoothness and efficiency in phenological estimation, Int J Appl Earth Obs, 47, 91-101, 440   https://doi.org/10.1016/j.jag.2015.11.009, 2016.

Qiu, B. W., Huang, Y. Z., Chen, C. C., Tang, Z. H., and Zou, F. L.: Mapping spatiotemporal dynamics of maize in China from 2005 to 2017 through designing leaf moisture based indicator from Normalized Multi-band Drought Index, Comput Electron Agr, 153, 82-93, https://doi.org/10.1016/j.compag.2018.07.039, 2018.

Sakamoto, T., Yokozawa, M., Toritani, H., Shibayama, M., Ishitsuka, N., and Ohno, H.: A crop phenology detection method 445   using time-series MODIS data, Remote Sens Environ, 96, 366-374, https://doi.org/10.1016/j.rse.2005.03.008, 2005.

Sakamoto, T., Wardlow, B. D., Gitelson, A. A., Verma, S. B., Suyker, A. E., and Arkebauer, T. J.: A Two-Step Filtering approach for detecting maize and soybean phenology with time-series MODIS data, Remote Sens Environ, 114, 2146-2159, https://doi.org/10.1016/j.rse.2010.04.019, 2010.

Sakamoto, T., Gitelson, A. A., and Arkebauer, T. J.: MODIS-based corn grain yield estimation model incorporating crop 450   phenology information, Remote Sens Environ, 131, 215-231, https://doi.org/10.1016/j.rse.2012.12.017, 2013.

Sakamoto, T.: Refined shape model fitting methods for detecting various types of phenological information on major US crops, Isprs J Photogramm, 138, 176-192, https://doi.org/10.1016/j.isprsjprs.2018.02.011, 2018.

Savitzky, A., and Golay, M. J. E.: Smoothing + Differentiation Of Data by Simplified Least Squares Procedures, Anal Chem, 36, 1627-&, https://doi.org/10.1021/ac60214a047, 1964.

455   Tao, F., Yokozawa, M., and Zhang, Z.: Modelling the impacts of weather and climate variability on crop productivity over a large area: A new process-based model development, optimization, and uncertainties analysis, Agr Forest Meteorol, 149, 831-850, https://doi.org/10.1016/j.agrformet.2008.11.004, 2009.

Tao, F. L., Yokozawa, M., Xu, Y. L., Hayashi, Y., and Zhang, Z.: Climate changes and trends in phenology and yields of field crops in China, 1981-2000, Agr Forest Meteorol, 138, 82-92, https://doi.org/10.1016/j.agrformet.2006.03.014, 2006.

460   Tao, F. L., Zhang, S. A., and Zhang, Z.: Spatiotemporal changes of wheat phenology in China under the effects of temperature, day length and cultivar thermal characteristics, Eur J Agron, 43, 201-212, https://doi.org/10.1016/j.eja.2012.07.005, 2012.

Tao, F. L., Zhang, Z., Shi, W. J., Liu, Y. J., Xiao, D. P., Zhang, S., Zhu, Z., Wang, M., and Liu, F. S.: Single rice growth period was prolonged by cultivars shifts, but yield was damaged by climate change during 1981-2009 in China, and late rice was just opposite, Global Change Biol, 19, 3200-3209, https://doi.org/10.1111/gcb.12250, 2013.

465   Tao, F. L., Zhang, S., Zhang, Z., and Rotter, R. P.: Maize growing duration was prolonged across China in the past three decades under the combined effects of temperature, agronomic management, and cultivar shift, Global Change Biol, 20, 3686-3699, https://doi.org/10.1111/gcb.12684, 2014.

Tao, J. B., Wu, W. B., Zhou, Y., Wang, Y., and Jiang, Y.: Mapping winter wheat using phenological feature of peak before winter on the North China Plain based on time-series MODIS data, J Integr Agr, 16, 348-359, https://doi.org/10.1016/S2095-
470   3119(15)61304-1, 2017.

Verger, A., Filella, I., Baret, F., and Penuelas, J.: Vegetation baseline phenology from kilometric global LAI satellite products, Remote Sens Environ, 178, 1-14, https://doi.org/10.1016/j.rse.2016.02.057, 2016.

Wang, C. Z., Zhang, Z., Chen, Y., Tao, F. L., Zhang, J., and Zhang, W.: Comparing different smoothing methods to detect double-cropping rice phenology based on LAI products - a case study in the Hunan province of China, Int J Remote Sens, 39,
475   6405-6428, https://doi.org/10.1080/01431161.2018.1460504, 2018.

Wang, H. S., Chen, J. S., Wu, Z. F., and Lin, H.: Rice heading date retrieval based on multi-temporal MODIS data and polynomial fitting, Int J Remote Sens, 33, 1905-1916, https://doi.org/10.1080/01431161.2011.603378, 2012.

Wang, N., Wang, J., Wang, E. L., Yu, Q., Shi, Y., and He, D.: Increased uncertainty in simulated maize phenology with more frequent supra-optimal temperature under climate warming, Eur J Agron, 71, 19-33, https://doi.org/10.1016/j.eja.2015.08.005,
480   2015.

Xiao, Z. Q., Liang, S. L., Wang, J. D., Chen, P., Yin, X. J., Zhang, L. Q., and Song, J. L.: Use of General Regression Neural Networks for Generating the GLASS Leaf Area Index Product From Time-Series MODIS Surface Reflectance, Ieee T Geosci Remote, 52, 209-223, https://doi.org/10.1109/Tgrs.2013.2237780, 2014.

Xiao, Z. Q., Liang, S. L., Wang, J. D., Xiang, Y., Zhao, X., and Song, J. L.: Long-Time-Series Global Land Surface Satellite
485   Leaf Area Index Product Derived From MODIS and AVHRR Surface Reflectance, Ieee T Geosci Remote, 54, 5301-5318, https://doi.org/10.1109/TGRS.2016.2560522, 2016.

Xu, X. M., Conrad, C., and Doktor, D.: Optimising Phenological Metrics Extraction for Different Crop Types in Germany Using the Moderate Resolution Imaging Spectrometer (MODIS), Remote Sens-Basel, 9, ARTN 254, https://doi.org/10.3390/rs9030254, 2017.

490 Yu, Y. Q., Huang, Y., and Zhang, W.: Changes in rice yields in China since 1980 associated with cultivar improvement, climate and crop management, Field Crop Res, 136, 65-75, https://doi.org/10.1016/j.fcr.2012.07.021, 2012.

Zeng, L. L., Wardlow, B. D., Wang, R., Shan, J., Tadesse, T., Hayes, M. J., and Li, D. R.: A hybrid approach for detecting corn and soybean phenology with time-series MODIS data, Remote Sens Environ, 181, 237-250, https://doi.org/10.1016/j.rse.2016.03.039, 2016.

495 Zhang, J. H., Feng, L. L., and Yao, F. M.: Improved maize cultivated area estimation over a large scale combining MODIS-EVI time series data and crop phenological information, Isprs J Photogramm, 94, 102-113, https://doi.org/10.1016/j.isprsjprs.2014.04.023, 2014a.

Zhang, S., and Tao, F. L.: Modeling the response of rice phenology to climate change and variability in different climatic zones: Comparisons of five models, Eur J Agron, 45, 165-176, https://doi.org/10.1016/j.eja.2012.10.005, 2013.

500 Zhang, S., Tao, F. L., and Zhang, Z.: Rice reproductive growth duration increased despite of negative impacts of climate warming across China during 1981-2009, Eur J Agron, 54, 70-83, https://doi.org/10.1016/j.eja.2013.12.001, 2014b.

Zhang, Z., Song, X., Chen, Y., Wang, P., Wei, X., and Tao, F. L.: Dynamic variability of the heading-flowering stages of single rice in China based on field observations and NDVI estimations, Int J Biometeorol, 59, 643-655, https://doi.org/10.1007/s00484-014-0877-6, 2015.

505 Zhao, Y., Bai, L. Y., Feng, J. Z., Lin, X. S., Wang, L., Xu, L. J., Ran, Q. Y., and Wang, K.: Spatial and Temporal Distribution of Multiple Cropping Indices in the North China Plain Using a Long Remote Sensing Data Time Series, Sensors-Basel, 16, ARTN 557, https://doi.org/10.3390/s16040557, 2016.

Zheng, H. B., Cheng, T., Yao, X., Deng, X. Q., Tian, Y. C., Cao, W. X., and Zhu, Y.: Detection of rice phenology through time series analysis of ground-based spectral index data, Field Crop Res, 198, 131-139, 510 https://doi.org/10.1016/j.fcr.2016.08.027, 2016.

Zhong, L. H., Hu, L. N., Yu, L., Gong, P., and Biging, G. S.: Automated mapping of soybean and corn using phenology, Isprs J Photogramm, 119, 151-164, https://doi.org/10.1016/j.isprsjprs.2016.05.014, 2016.

Zhou, G. X., Liu, X. N., and Liu, M.: Assimilating Remote Sensing Phenological Information into the WOFOST Model for Rice Growth Simulation, Remote Sens-Basel, 11, ARTN 268, https://doi.org/10.3390/rs11030268, 2019.

515 Zhu, W. Q., Pan, Y. Z., He, H., Wang, L. L., Mou, M. J., and Liu, J. H.: A Changing-Weight Filter Method for Reconstructing a High-Quality NDVI Time Series to Preserve the Integrity of Vegetation Phenology, Ieee T Geosci Remote, 50, 1085-1094, https://doi.org/10.1109/Tgrs.2011.2166965, 2012.

520 **Table 1: Mean RMSE (in parenthesis) of the most suitable smoothing method for different regions and crops.**

Province	Winter wheat	Spring wheat	Summer maize	Spring maize	Single-rice	Double rice
Anhui	SG-3 (3.53)		SG-4 (6.81)		SG-5 (5.67)	SG-3 (6.69)
Beijing	SG-3 (5.46)		SG-3 (8.06)			
Chongqing	SG-3 (7.09)			SG-3 (8.06)	SG-3 (3.46)	
Fujian	SG-3 (8.90)				SG-3 (6.36)	SG-3 (6.02)
Gansu	SG-3 (5.43)	SG-3 (7.69)	SG-5 (7.63)	SG-3 (8.34)		
Guangdong						SG-3 (6.38)
Guangxi				SG-3 (8.17)		SG-3 (7.25)
Guizhou	SG-3 (6.59)		SG-3 (9.77)	SG-3 (9.11)	SG-3 (7.62)	
Hainan						db8 (2.33)
Hebei	SG-3 (4.53)	SG-3 (6.35)	SG-3 (4.58)	SG-3 (5.42)	SG-3 (6.32)	
Heilongjiang		SG-5 (6.38)		SG-5 (6.72)	SG-5 (4.73)	
Henan	SG-3 (4.22)		SG-4 (5.01)		SG-5 (3.48)	
Hubei	SG-3 (5.65)			SG-3 (7.89)	SG-3 (5.87)	SG-3 (5.89)
Hunan				SG-3 (8.10)	SG-3 (5.03)	SG-3 (7.64)
Jiangsu	SG-3 (5.12)		SG-4 (6.44)	db4 (8.67)	SG-5 (6.85)	
Jiangxi				SG-3 (7.95)	SG-3 (7.80)	SG-3 (8.12)
Jilin		SG-4 (7.73)		SG-5 (5.84)	SG-5 (6.30)	
Liaoning				SG-3 (4.91)	SG-3 (6.39)	
Inner Mongolia		SG-3 (7.85)		SG-5 (5.55)		
Ningxia	SG-3 (6.18)	SG-3 (6.74)	SG-3 (7.50)	SG-5 (6.33)	SG-5 (8.22)	
Qinghai	db3 (6.73)	DL (7.56)		SG-5 (7.59)		
Shandong	SG-3 (4.46)		SG-4 (4.55)		SG-5 (6.36)	
Shanghai	SG-3 (5.01)				SG-3 (7.15)	
Shannxi	SG-3 (4.04)	SG-3 (8.08)	SG-3 (4.09)	SG-3 (5.05)	SG-5 (7.57)	
Shanxi	SG-3 (4.61)	DL (7.90)	SG-3 (5.45)	SG-5 (5.57)	SG-5 (8.84)	
Sichuan	SG-3 (5.43)		SG-3 (7.43)	SG-3 (7.84)	SG-3 (5.51)	
Tianjin	SG-3 (7.36)		SG-3 (8.17)			
Xinjiang	SG-3 (6.93)	SG-3 (7.99)	SG-3 (7.11)	SG-3 (6.14)		
Xizang	SG-3 (7.02)	SG-3 (7.12)				
Yunnan	SG-3 (7.53)		SG-3 (8.45)	SG-3 (8.19)	SG-5 (7.53)	SG-3 (4.51)
Zhejiang	SG-3 (6.22)				SG-3 (6.35)	SG-4 (7.33)

Table 2: Mean RMSE between retrieved phenological dates and phenological observations.

Crop	Stage	RMSE (days)	Error ≤ ±10 days (%)	Error ⩾ ±10 days (%)	R^2
Rice	Transplanting	4.05	98.6%	1.4%	
	Heading	5.59	93.0%	7.0%	0.98
	Maturity	6.21	88.9%	11.1%	
Wheat	Green up & Emergence	2.82	99.5%	0.5%	
	Heading	6.54	86.4%	13.6%	0.97
	Maturity	7.18	81.7%	18.3%	
Maize	V3	4.08	96.8%	3.2%	
	Heading	7.79	79.8%	20.2%	0.97
	Maturity	8.22	71.8%	28.2%	

Table 3: Annual mean phenological dates and growth periods of different crops in each sub-region

Crop	Stage (period)	Sub-region				
		I	II	III	IV	V
Early rice	Transplanting (VGP)			115.4 (60)		99 (69.3)
	Heading (RGP)			175.2 (20.4)		168.2 (27.6)
	Maturity (GP$_w$)			195.1 (79.7)		195.5 (96.6)
Late rice	Transplanting (VGP)			204.2 (48.1)		209.4 (54.1)
	Heading (RGP)			252.2 (35.5)		265.7 (46.5)
	Maturity (GP$_w$)			287.7 (83.5)		310 (100.6)
Single rice	Transplanting (VGP)	141.7 (75.5)	154.1 (64.2)	158.5 (62.5)	130.4 (76.6)	
	Heading (RGP)	217.2 (37.9)	218.3 (37.1)	221 (43.7)	207 (53.4)	
	Maturity (GP$_w$)	255 (113.5)	255.3 (101)	264.6 (106)	260.4 (130)	
Wheat	Green up & Emergence (VGP)	128 (65.1)	51.8 (62.9)	108.7 (57.5)	29.6 (34.7)	
	Heading (RGP)	187.6 (41.1)	113.9 (29.6)	165.7 (63.7)	72.3 (57.1)	
	Maturity (GP$_w$)	224.8 (106)	143.3 (92.5)	228.8 (121)	128.7 (91.7)	
Spring maize	V3 (VGP)	142.4 (71.9)		130.2 (79.6)	104.3 (74.5)	
	Heading (RGP)	214.3 (40.6)		209.9 (42.2)	178.8 (59.7)	
	Maturity (GP$_w$)	254.9 (113)		252.1 (122)	238.5 (134)	
Summer maize	V3 (VGP)		173.1 (46.9)	179.1 (47.1)	129.3 (74.1)	
	Heading (RGP)		220.1 (37.5)	226.2 (36.1)	203.3 (53.3)	
	Maturity (GP$_w$)		257.5 (84.5)	262.2 (83.1)	256.6 (127)	

Note: VGP means vegetative growth period, the difference between heading and transplanting/Green up & Emergence/V3 dates; RGP means reproductive growth period, the difference between maturity and heading dates; GP$_w$ means whole growth period, the difference between maturity and transplanting/Green up & Emergence/V3 dates. The numbers in the parentheses mean the annual mean growth periods.

 Table 4: The trend (days year^{-1}) of three key phenological dates and growth periods from 2000 to 2015

Crop	Stage (period)	Sub-region									
		I		II		III		IV		V	
		Trend	Psg	Trend	Psg	Trend	Psg	Trend	Psg	Trend	Psg
Early rice	Transplanting					-0.7	27.8			-0.8	27.3
	(VGP)					(0.6)	(19.8)			(1.5)	(11.8)
	Heading					-0.8	26.1			1.3	29.1
	(RGP)					(1.3)	(15.5)			(1.0)	(14.5)
	Maturity					0.7	23.3			1.6	29.6
	(GP$_w$)					(1.3)	(19.4)			(1.7)	(14.3)
Late rice	Transplanting					0.7	25.4			1.7	28.2
	(VGP)					(0.01)	(15.6)			(0.01)	(44.3)
	Heading					0.7	31.1			1.7	29.1
	(RGP)					(1.0)	(16.5)			(2.2)	(13.7)
	Maturity					1.1	32.6			2.4	35.4
	(GP$_w$)					(1.1)	(15.8)			(2.3)	(13.4)
Single rice	Transplanting	0.01	31.6	-1.1	43.3	0.01	37.9	-1.3	22.3		
	(VGP)	(-0.01)	(29.3)	(1.3)	(31.6)	(0.8)	(22.9)	(1.3)	(13.5)		
	Heading	0.01	38.7	0.01	32.4	0.7	31.6	-0.01	19.1		
	(RGP)	(0.7)	(20.1)	(0.7)	(18.1)	(0.8)	(16.8)	(1.8)	(17.6)		
	Maturity	0.7	20	0.7	28.2	1	28.5	1.6	24.1		
	(GP$_w$)	(0.6)	(14.8)	(1.7)	(29.8)	(1.2)	(22.1)	(2.1)	(19.7)		
Wheat	Green up & Emergence	0.01	61.6	0.6	16.9	1.2	15	1.7	26.5		
	(VGP)	(-1.5)	(22.2)	(-0.4)	(12.8)	(-0.9)	(14.1)	(-2.0)	(12.1)		
	Heading	-0.01	34.6	0.6	21.9	0.9	23.4	0.8	35		
	(RGP)	(0.01)	(13.1)	(-0.6)	(14.9)	(-0.8)	(12.7)	(2.3)	(14.8)		
	Maturity	0.01	30.3	0.01	22.1	1.4	17.3	1.9	42.8		
	(GP$_w$)	(-1.9)	(17.4)	(-0.7)	(12.1)	(-1.2)	(12.4)	(1.7)	(11.2)		
Spring maize	V3	0.01	26.2			-1.1	20.4	-1.0	33.6		
	(VGP)	(-0.9)	(20.9)			(1.2)	(12.6)	(-1.3)	(15.1)		
	Heading	-0.01	54.8			0.01	55.4	-1.4	28.9		
	(RGP)	(0.9)	(20.1)			(0.9)	(12.8)	(2.0)	(16.5)		

	Maturity	0.01	26.4			-0.5	31.4	0.7	31.3
	(GP$_w$)	(-0.7)	(13.9)			(1.4)	(11.8)	(1.5)	(14.6)
Summer maize	V3			0.01	52.6	-0.9	27.6	-0.01	41.2
	(VGP)			(-0.7)	(22.1)	(-1.0)	(12.1)	(1.2)	(11.8)
	Heading			0.4	27.3	-0.01	30.1	0.01	40.1
	(RGP)			(-0.8)	(13.4)	(0.01)	(13.2)	(2.3)	(19.1)
	Maturity			0.4	20.1	-1.4	34.7	2.4	48.8
	(GP$_w$)			(-1.0)	(16.7)	(-1.1)	(12.9)	(2.5)	(18.3)

Note: The same meanings for VGP, RGP and GP$_w$ as Table 3; Psg (%) means the percent of grids showing significant trend at $p<0.1$ level; The numbers in the parentheses mean the statistic values of grids during three growth periods.
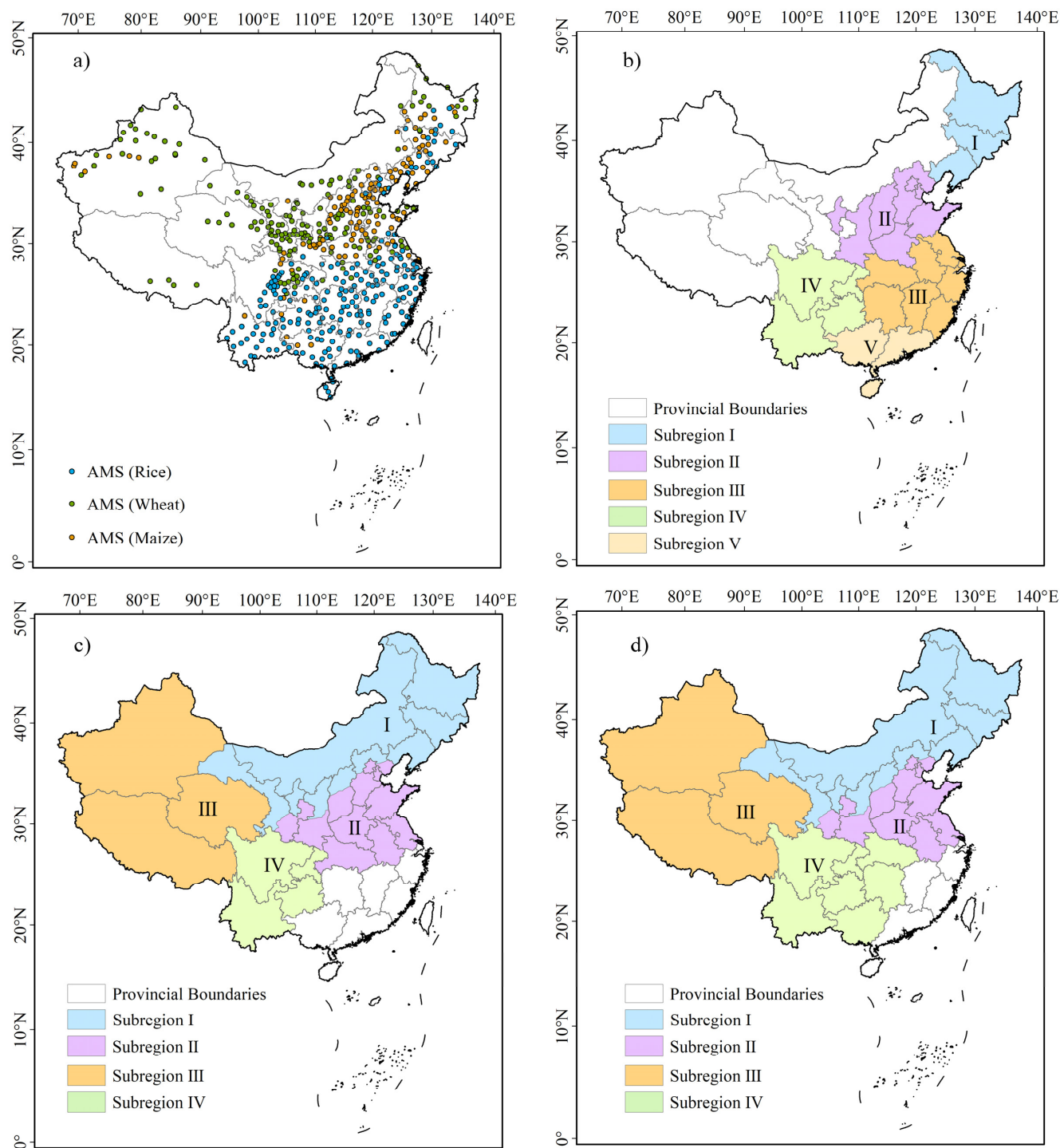
Fig.1: The spatial distribution of Agricultural Meteorological Stations (AMS) in studied areas (a) and the locations of divided subregions for rice (b), wheat (c), and maize(d).
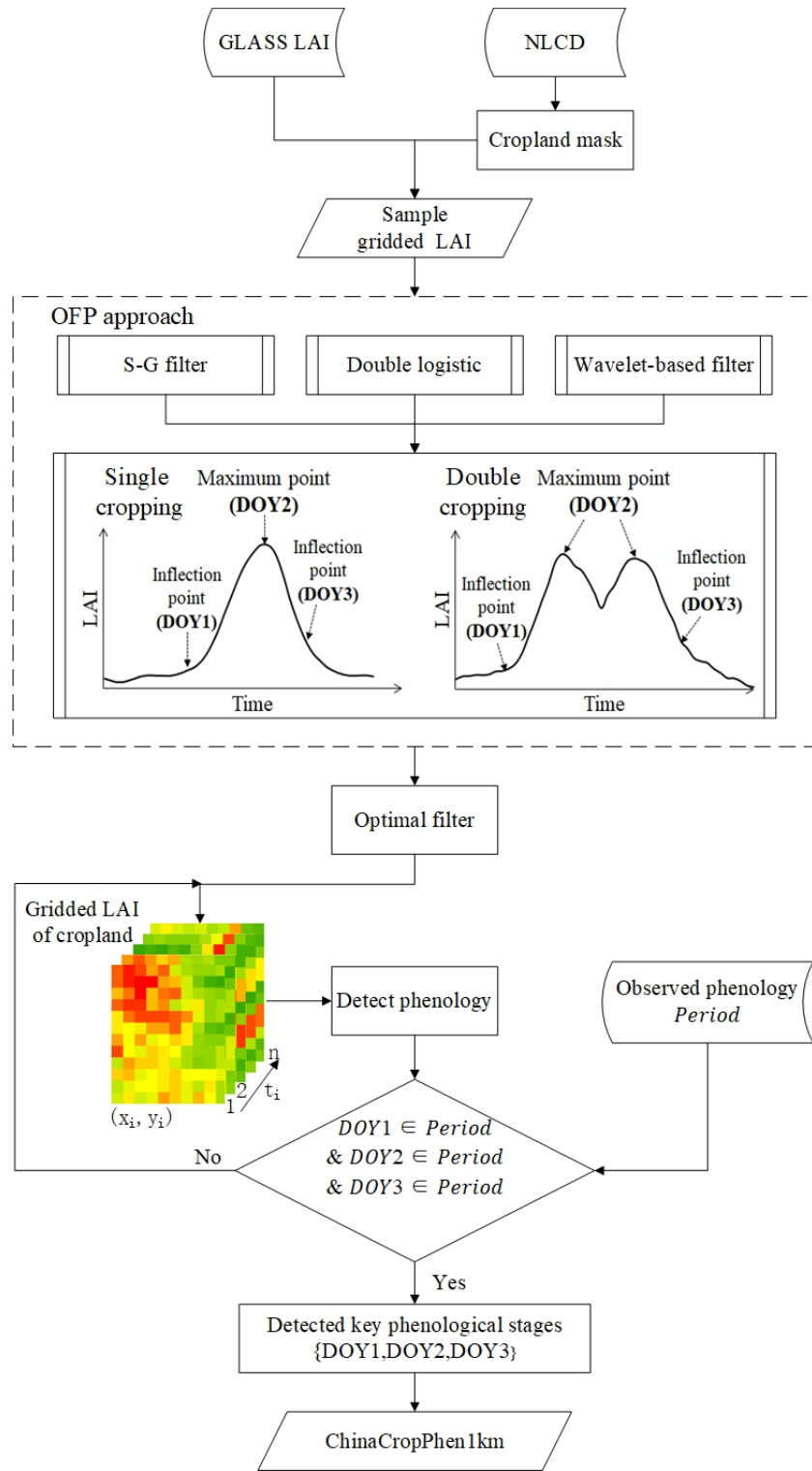
Fig.2: Flow chart of procedures for data analysis and crop phenological dates identification.
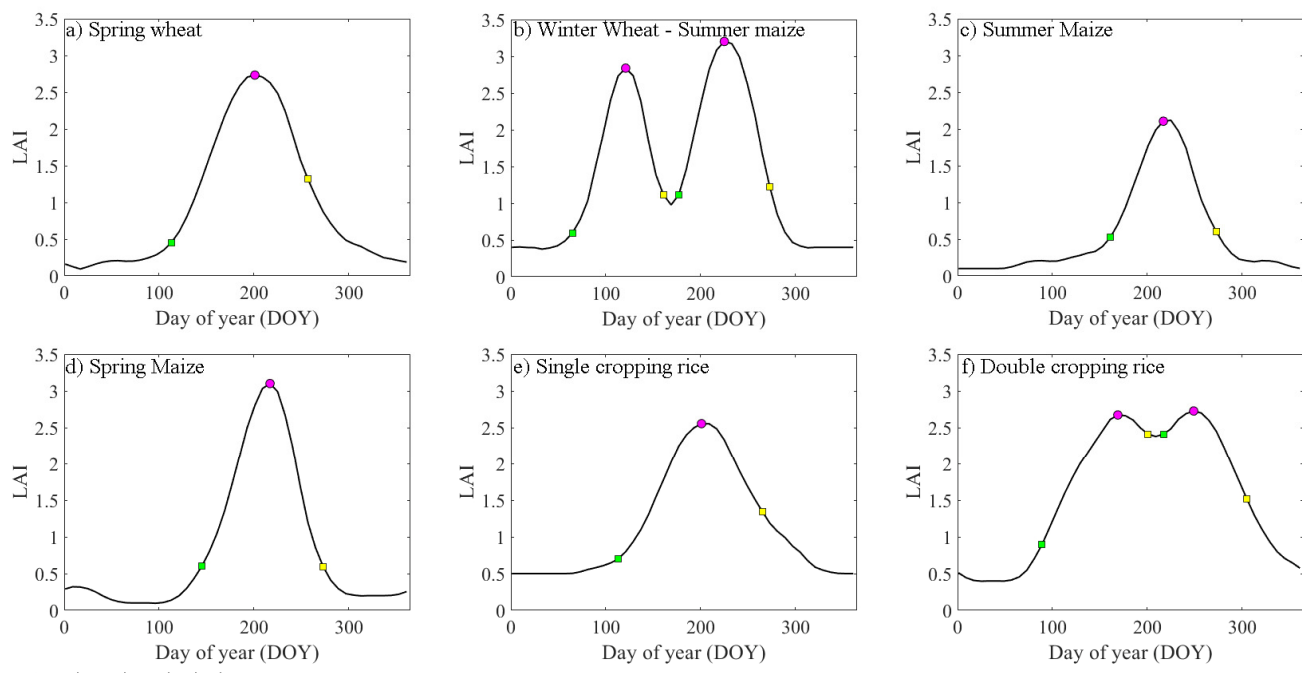
540

Fig.3: Typical phenological curves for different crop cropping systems in China.
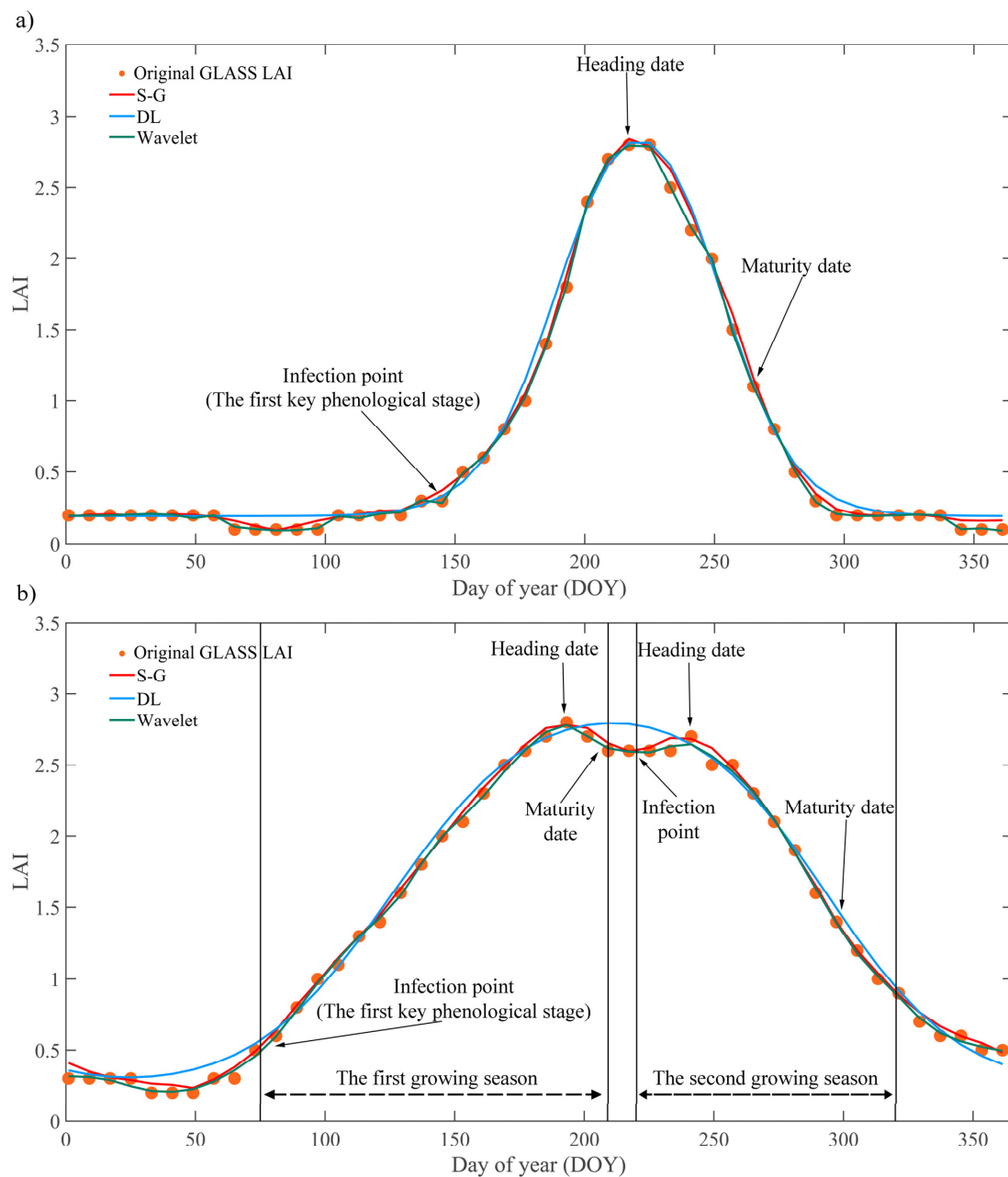
Fig.4: Comparisons of different smoothing methods for different cropping systems.

545
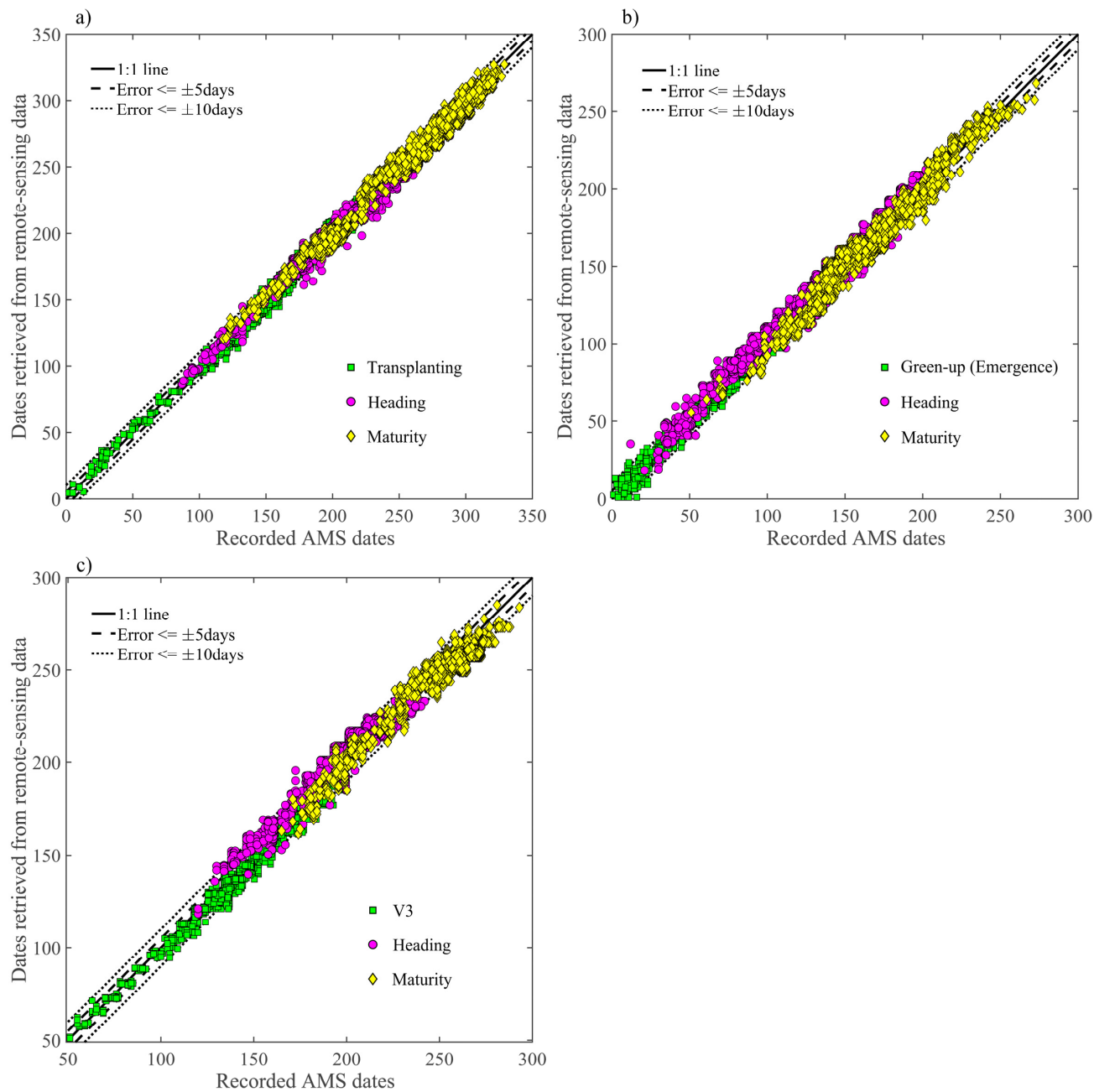
Fig.5: Comparisons between retrieved and observed phenological dates for rice (a), wheat (b), and maize (c).
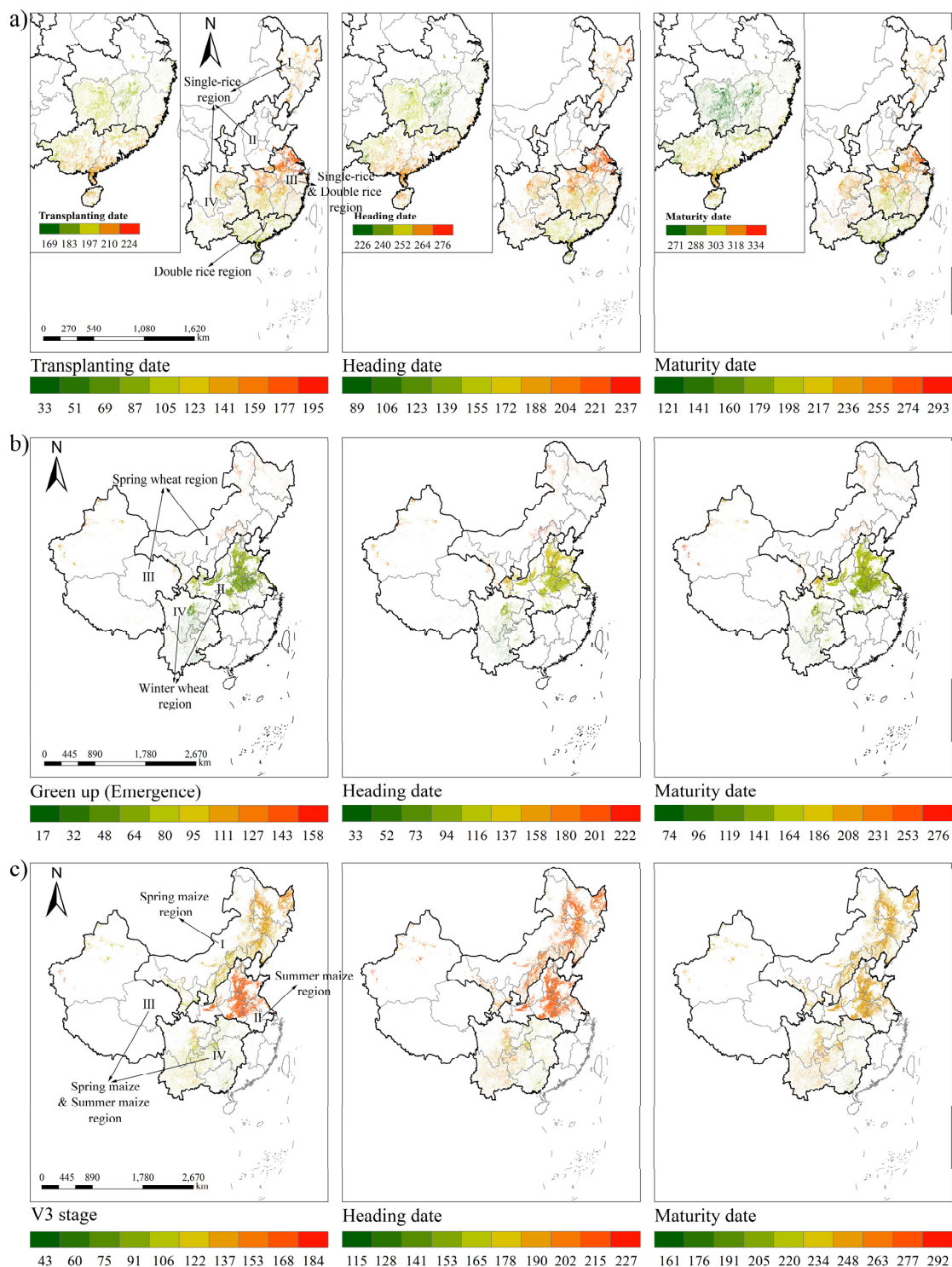
Fig.6: Spatial patterns of annual averages of three key phenological dates during 2000~2015 for rice (a), wheat (b), and maize (c).
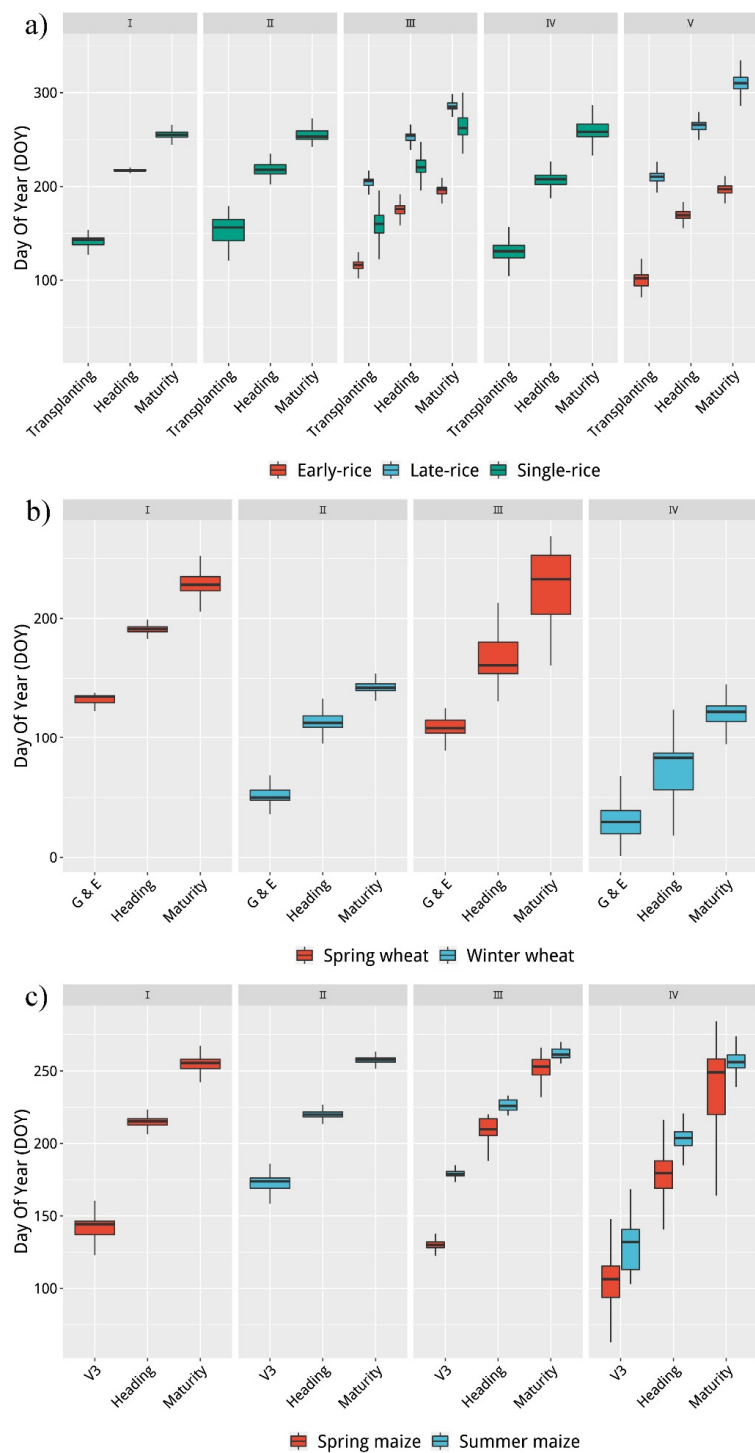
Fig.7: Box plots of three key phenological dates by crop and sub-regions during 2000~2015 for rice (a), wheat (b), and maize (c).

550
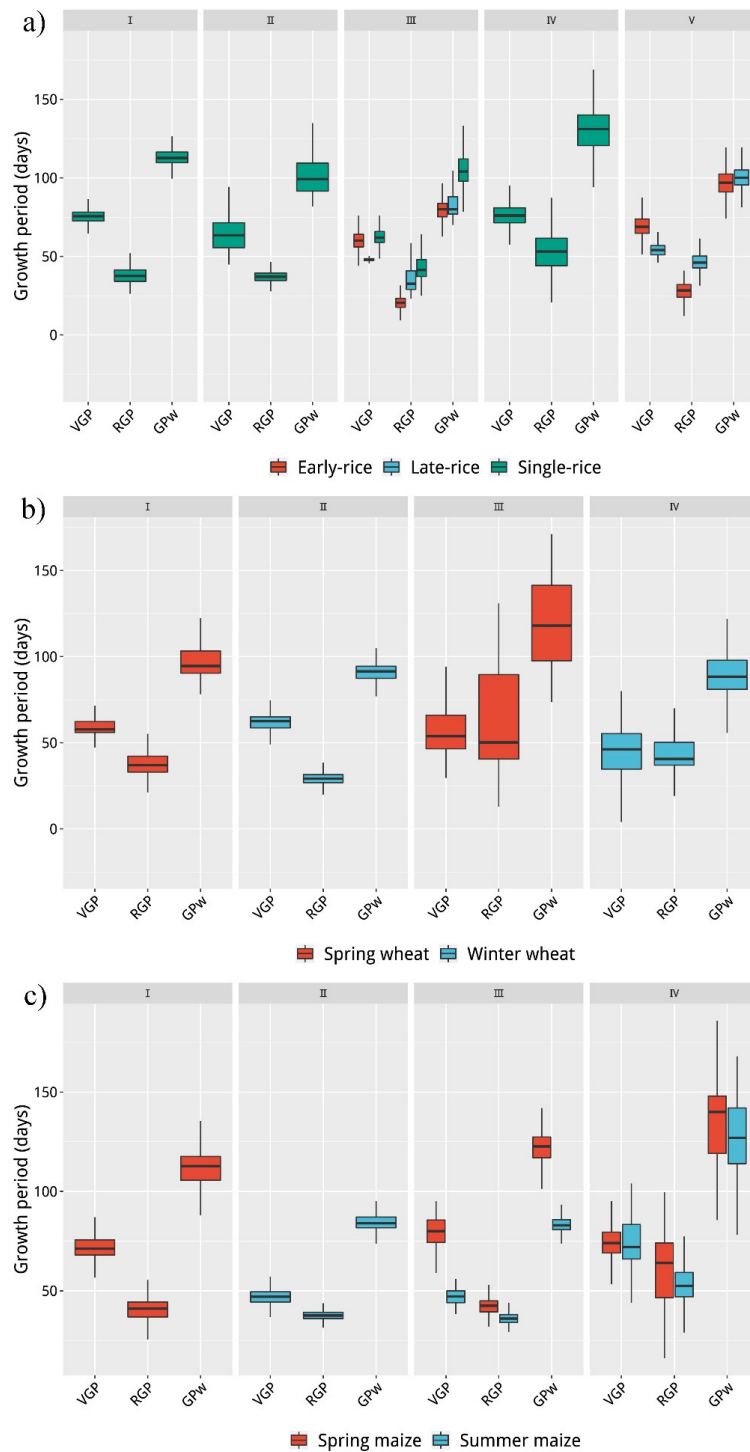
Fig.8: Box plots of three key phenological periods by crop and sub-regions during 2000~2015, for vegetative growth period (VGP), reproductive growth period (VGP), and whole growth period (GPW) of rice (a), wheat (b), and maize (c).

555
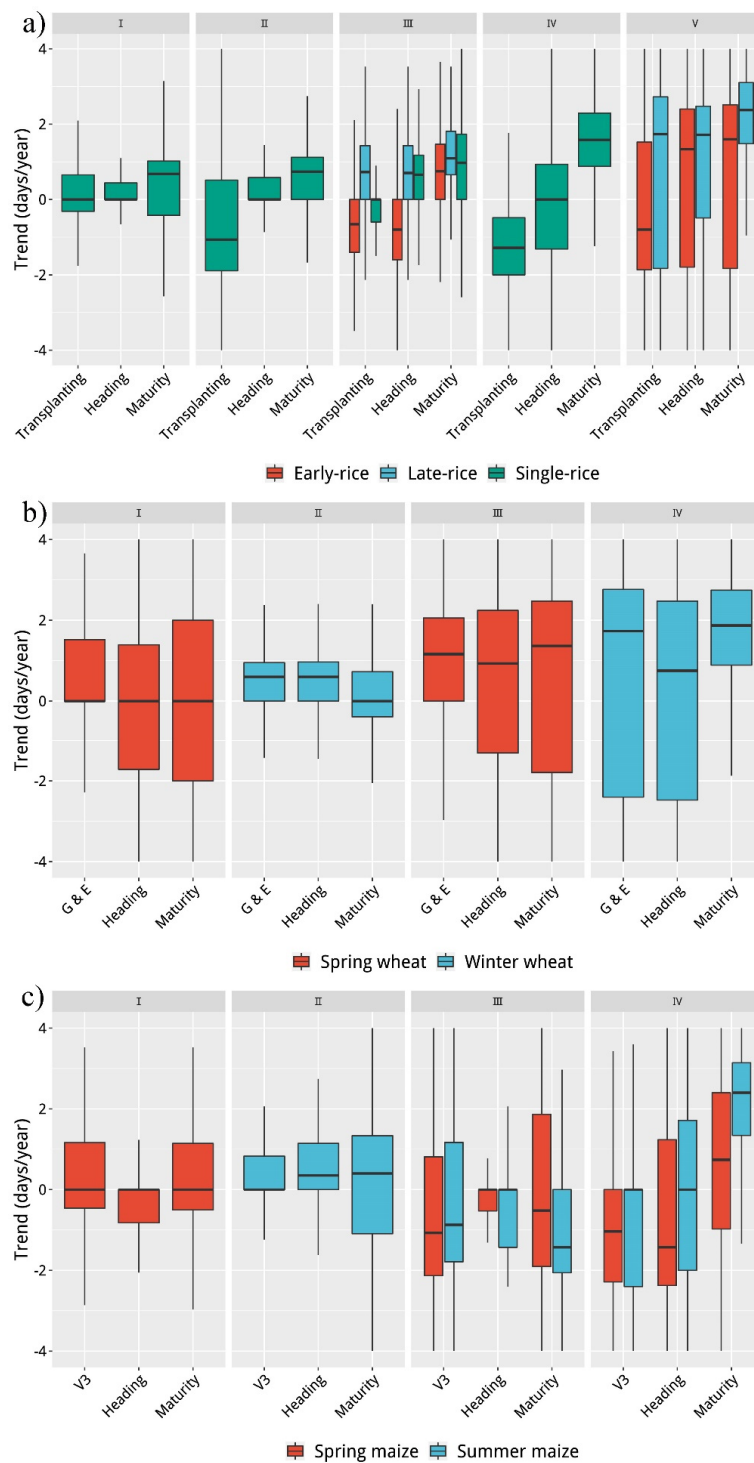
Fig.9: The trends of three key phenological dates during 2000~2015 by crop and sub-regions for rice (a), wheat (b), and maize (c).
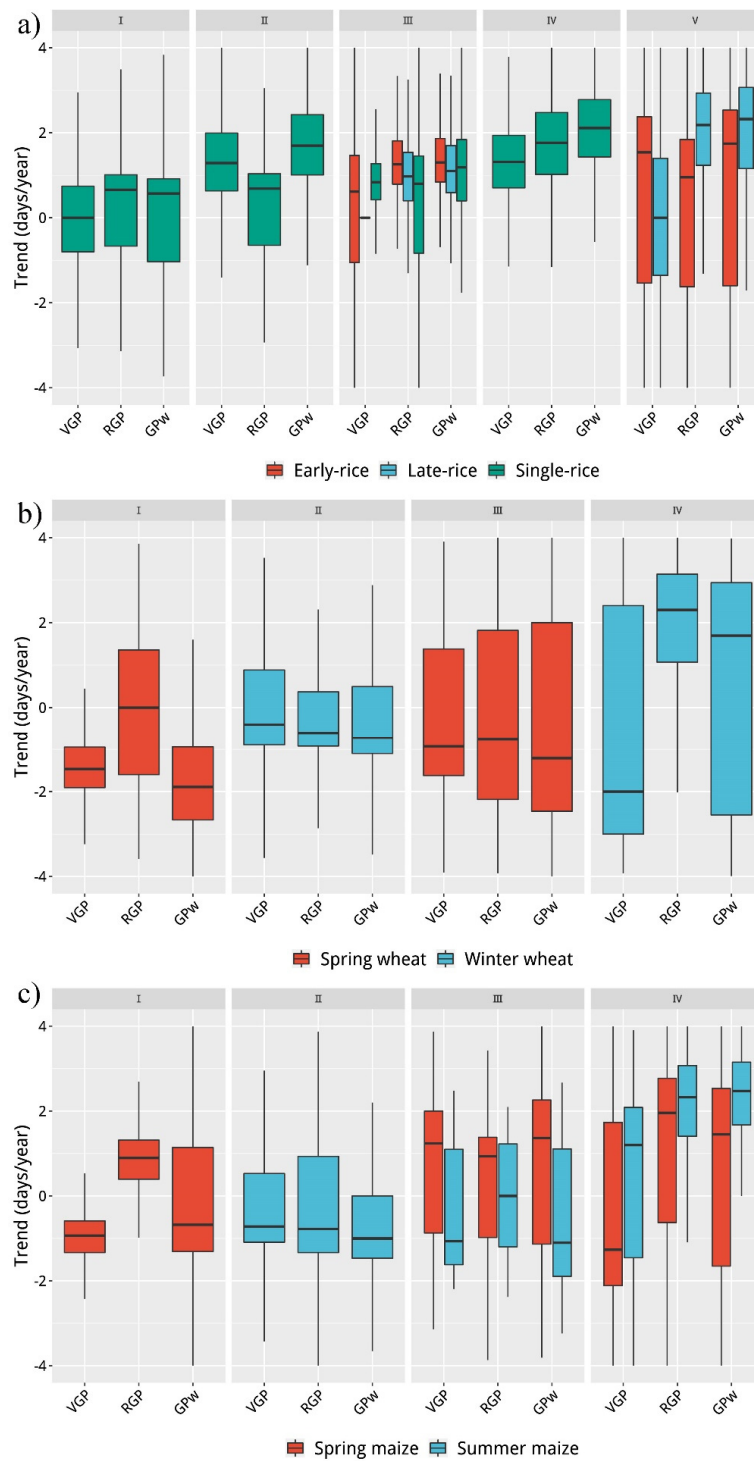
Fig.10: The trends of three key phenological periods during 2000~2015 by crop and sub-regions, VGP for vegetative growth period, RGP for reproductive growth period, and GPW for whole growth period of rice (a), wheat (b), and maize (c).